

Enhancement-mode PEDOT:PSS organic electrochemical transistors using molecular de-doping

Citation for published version (APA):

Keene, S. T., van der Pol, T. P. A., Zakhidov, D., Weijtens, C. H. L., Janssen, R. A. J., Salleo, A., & van de Burgt, Y. (2020). Enhancement-mode PEDOT:PSS organic electrochemical transistors using molecular de-doping. *Advanced Materials*, 32(19), Article 2000270. <https://doi.org/10.1002/adma.202000270>

Document license:
CC BY

DOI:
[10.1002/adma.202000270](https://doi.org/10.1002/adma.202000270)

Document status and date:
Published: 01/05/2020

Document Version:
Publisher's PDF, also known as Version of Record (includes final page, issue and volume numbers)

Please check the document version of this publication:

- A submitted manuscript is the version of the article upon submission and before peer-review. There can be important differences between the submitted version and the official published version of record. People interested in the research are advised to contact the author for the final version of the publication, or visit the DOI to the publisher's website.
- The final author version and the galley proof are versions of the publication after peer review.
- The final published version features the final layout of the paper including the volume, issue and page numbers.

[Link to publication](#)

General rights

Copyright and moral rights for the publications made accessible in the public portal are retained by the authors and/or other copyright owners and it is a condition of accessing publications that users recognise and abide by the legal requirements associated with these rights.

- Users may download and print one copy of any publication from the public portal for the purpose of private study or research.
- You may not further distribute the material or use it for any profit-making activity or commercial gain
- You may freely distribute the URL identifying the publication in the public portal.

If the publication is distributed under the terms of Article 25fa of the Dutch Copyright Act, indicated by the "Taverne" license above, please follow below link for the End User Agreement:

www.tue.nl/taverne

Take down policy

If you believe that this document breaches copyright please contact us at:

openaccess@tue.nl

providing details and we will investigate your claim.

Enhancement-Mode PEDOT:PSS Organic Electrochemical Transistors Using Molecular De-Doping

Scott T. Keene, Tom P. A. van der Pol, Dante Zakhidov, Christ H. L. Weijtens, René A. J. Janssen, Alberto Salleo,* and Yoeri van de Burgt*

Organic electrochemical transistors (OECTs) show great promise for flexible, low-cost, and low-voltage sensors for aqueous solutions. The majority of OECT devices are made using the polymer blend poly(ethylenedioxythiophene):poly(styrene sulfonate) (PEDOT:PSS), in which PEDOT is intrinsically doped due to inclusion of PSS. Because of this intrinsic doping, PEDOT:PSS OECTs generally operate in depletion mode, which results in a higher power consumption and limits stability. Here, a straightforward method to de-dope PEDOT:PSS using commercially available amine-based molecular de-dopants to achieve stable enhancement-mode OECTs is presented. The enhancement-mode OECTs show mobilities near that of pristine PEDOT:PSS ($\approx 2 \text{ cm}^2 \text{ V}^{-1} \text{ s}^{-1}$) with stable operation over 1000 on/off cycles. The electron and proton exchange among PEDOT, PSS, and the molecular de-dopants are characterized to reveal the underlying chemical mechanism of the threshold voltage shift to negative voltages. Finally, the effect of the de-doping on the microstructure of the spin-cast PEDOT:PSS films is investigated.

changes in a transistor structure, typically called an organic electrochemical transistor (OECT) (Figure 1a).^[15] OECTs operate within relatively small voltage windows ($\pm 1 \text{ V}$ vs Ag/AgCl) with high transconductance (g_m), which is a result of their volumetric doping/de-doping when gated with an electrolyte solution.^[16,17] Typically, OECTs utilize the polymer blend of poly(ethylenedioxythiophene):poly(styrene sulfonate) (PEDOT:PSS) exploiting its high electronic and ionic mobilities ($\approx 1\text{--}2 \text{ cm}^2 \text{ V}^{-1} \text{ s}^{-1}$ and $1 \times 10^{-3} \text{ cm}^2 \text{ V}^{-1} \text{ s}^{-1}$, respectively),^[18,19] high transconductance (g_m),^[20] ease of processing, and commercial availability. PEDOT:PSS achieves mixed conducting behavior by blending two polymers which act, broadly speaking, as the electronic (PEDOT) and ionic (PSS) conducting materials.

Organic mixed ionic/electronic conductor (OMIEC) materials have recently shown promise as the active material in a wide range of bioelectronic devices and applications, including flexible biosensors,^[1–4] electrophysiological recording electrodes,^[5–8] cell monitoring,^[9–11] and neuromorphic computing.^[12–14] OMIECs are of interest because they can convert ionic inputs into conductivity


Although PEDOT:PSS performs exceptionally well as an OECT,^[21] one of its main drawbacks is that it operates in depletion mode; the transistor channel is initially doped (conductive) and a gate voltage must be applied to lower the channel conductivity. This intrinsic doping leads to high operating currents ($\approx \text{mA}$) and requires the use of a high static gate voltage ($V_G \approx +0.8 \text{ V}$ vs Ag/AgCl) to keep the device in its off state. This high V_G can lead to instability for devices operated in an aqueous electrolyte and often results in parasitic reactions with water and oxygen^[22,23] leading to device degradation. Instead, enhancement-mode devices which have negative threshold voltages^[24,25] (V_{th}) would help mitigate these issues. Thus, it would be favorable to shift the operating voltage range for PEDOT:PSS OECTs to lower the channel current, leading to reduced power consumption when implemented in bioelectronic systems, as well as to avoid parasitic reactions.

The operating voltage range of OECTs have previously been tuned by utilizing vapor de-doping with polyethyleneimine (PEI),^[12,23,26] altering the gate to a high reduction potential redox couple,^[27] or by synthesizing entirely new polymer channel materials.^[28] However, each of these processes falls short for simple fabrication and scalability of OECT and other OMIEC based devices. PEI vapor de-doping results in high device-to-device variance and would require an additional time-consuming chemical vapor deposition step. In addition, we have previously shown that vapor deposited PEI is susceptible to leaching out leading to poor device stability.^[23] Changing the gate electrode changes the voltage between the gate and

S. T. Keene, D. Zakhidov, A. Salleo
Department of Materials Science and Engineering
Stanford University
Stanford, CA 94305, USA
E-mail: asalleo@stanford.edu

T. P. A. van der Pol, C. H. L. Weijtens, R. A. J. Janssen
Molecular Materials and Nanosystems and Institute
for Complex Molecular Systems
Eindhoven University of Technology
Eindhoven 5612AJ, Netherlands

Y. van de Burgt
Microsystems and Institute for Complex Molecular Systems
Eindhoven University of Technology
Eindhoven 5612AJ, Netherlands
E-mail: y.b.v.d.burgt@tue.nl

 The ORCID identification number(s) for the author(s) of this article can be found under <https://doi.org/10.1002/adma.202000270>.

© 2020 The Authors. Published by WILEY-VCH Verlag GmbH & Co. KGaA, Weinheim. This is an open access article under the terms of the Creative Commons Attribution License, which permits use, distribution and reproduction in any medium, provided the original work is properly cited.

DOI: 10.1002/adma.202000270

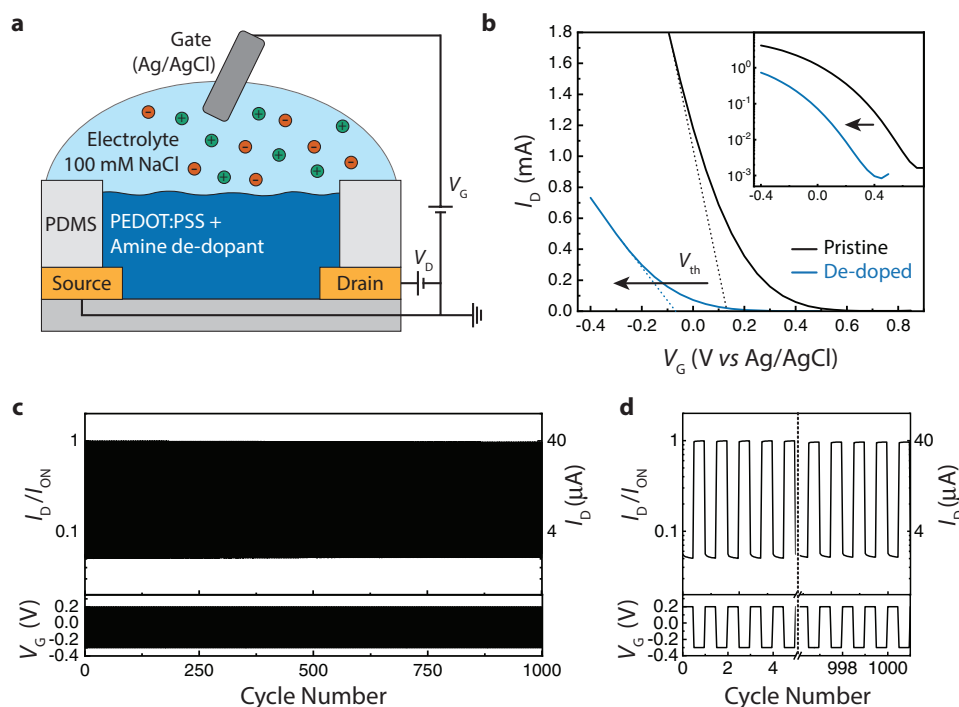


Figure 1. Effect of amine de-doping on organic electrochemical transistor (OECT) operating voltage and stability. a) Schematic showing OECT device configuration and b) representative transfer curves of pristine (black) and de-doped (blue) PEDOT:PSS OECTs. c) Stability of the de-doped OECT for 1000 on/off cycles with d) a close-up comparing the first and last five cycles.

channel but does not alter the relative potentials with respect to ambient oxygen and water, and thus the channel material would still exhibit parasitic reactions. Developing new channel materials is promising, but new water-stable electrochemically active polymers are not yet commercially available while PEDOT:PSS has been developed commercially for over two decades. Ideally, the operating voltage range for PEDOT:PSS OECTs could be directly modified using commercially available materials without affecting the device performance. Recently, aliphatic amines have been demonstrated to efficiently reduce PEDOT:PSS via a cascading reaction of electrons and protons donated from the amine.^[29] The ability of these amines to change the doping state in PEDOT:PSS makes them interesting candidates for tuning the operating voltage of PEDOT:PSS OECTs.

In this work, we use aliphatic amine de-dopant molecules to demonstrate enhancement-mode PEDOT:PSS OECTs cast from a single aqueous solution (Figure 1a,b). The resulting devices show a shift in the V_{th} by approx. -0.35 V and a decreased source-drain current (I_{SD}) by a factor of $15\text{--}20\times$ at $V_G = 0$ V versus Ag/AgCl (Figure 1b), reducing the operating currents of the transistor. Importantly, the devices show stable device operation for over 1000 on/off cycles (Figure 1c,d), which is a significant improvement compared to PEI de-doped devices which suffer from cycling instability.^[23] We uncover the underlying chemical mechanisms that cause the shift in operating voltage of de-doped PEDOT:PSS OECTs. Then, we investigate the effect of de-dopant concentration and molecular structure on the device performance metrics and materials microstructure to optimize the performance of PEDOT:PSS enhancement-mode OECTs.

To understand how molecular de-doping affects the device performance, we fabricated OECTs using PEDOT:PSS dispersion mixed with either diethylenetriamine (DETA), *N*-methyl-2,2'-diaminodiethylamine (DEMTA), or tris(aminoethyl) amine (TAEA) at concentrations ranging from 4.8% v/v to 50% v/v (see Experimental Section). These de-doping agents were selected due to their inclusion of a structural motif required for strong de-doping as described in previous work^[29] as well as their compatibility with the aqueous PEDOT:PSS dispersion (see Text S1, Supporting Information). The thickness-normalized transfer curves (Figure 2a–c) show that all de-doped PEDOT:PSS channels can be operated as enhancement-mode OECTs with threshold voltages just below 0 V ranging from approx. -5 to -100 mV. The transfer curves are normalized by thickness in order to more accurately compare the materials properties rather than the device properties (e.g., transconductance and conductance) which are thickness dependent. From the transfer curves of five samples at each concentration, we quantify the average V_{th} and thickness-normalized peak transconductance (at $V_{DS} = -0.6$ V, $W L^{-1} = 1$) g_m/t for each de-doping concentration and find no correlation with the de-dopant concentration in the range between 4.8% v/v and 50% v/v (Figure 2d). To compare the performance of de-doped PEDOT:PSS channels, we measured the conductivity of both the as de-doped film (Figure 2e) and the film that was electrochemically cycled from 0.5 to -0.4 V, and back to 0.5 V versus Ag/AgCl (Figure 2f). As expected, we observed a large decrease in the “as de-doped” film conductivity ($\approx 10^2\times$ to $10^3\times$ decrease) due to the lower carrier concentration as the de-dopant concentration is increased. In contrast, the cycled films did not show a strong dependence between de-dopant concentration and conductivity, with all conductivity values

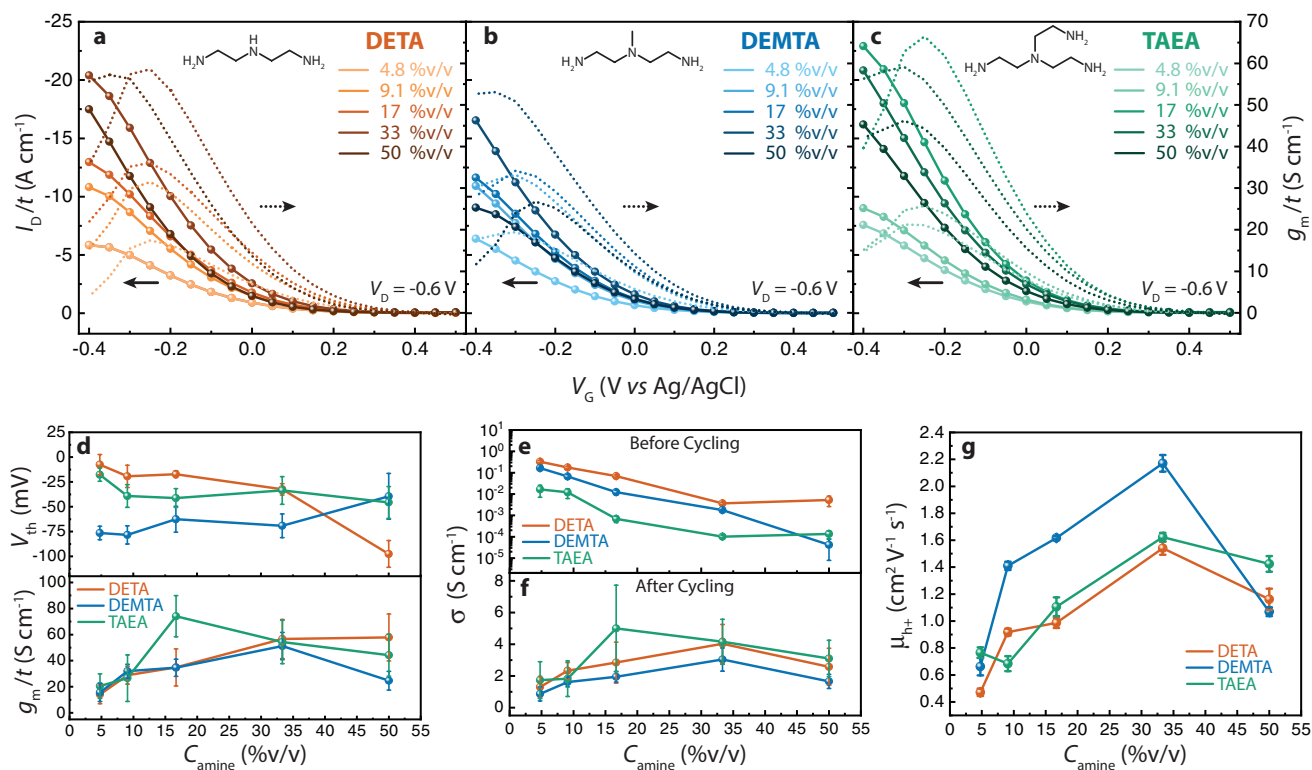


Figure 2. Organic electrochemical transistor (OECT) device characteristics using de-doped PEDOT:PSS as the channel material. a–c) Thickness normalized transfer characteristics for PEDOT:PSS channels de-doped with varied concentrations of DETA (a), DEMA (b), and TAEA (c) operated in the saturation regime using a drain source voltage of -0.6 V taken from the fourth operation cycle. Source-drain current I_d is plotted with solid lines and symbols (left y-axis) and the thickness-normalized transconductance g_m/t is plotted with dotted lines (right y-axis). d) Threshold voltage V_{th} and peak g_m/t extracted from the OECT transfer characteristics. e, f) Conductivity of devices before (e) and after (f) electrochemical cycling of the device to the on state and back to the off state. g) Comparison of mobilities of de-doped PEDOT:PSS films using a current pulsed technique (ref. [30], see Figure S1, Supporting Information). Values and error bars in (d)–(g) are the resulting average and standard deviation, respectively, from measuring five individual devices.

between ≈ 1 – 5 S cm⁻¹. We also compared the hole mobility (μ_{h+}) (Figure 2g), which was measured using a previously reported current pulsing technique^[30] (see Figure S1, Supporting Information). Interestingly, μ_{h+} increases with increasing de-dopant concentration up to 33% v/v for all molecules used, with peak mobilities in the range of 1–2 cm² V⁻¹ s⁻¹, approaching that of pristine PEDOT:PSS devices, which were measured to be ≈ 4.5 cm² V⁻¹ s⁻¹. These results confirm the effectiveness of amine de-doping to lower V_{th} while retaining near-pristine mobilities. To understand the similarity in V_{th} for each of the three amines across a wide range of concentrations, we investigated the origin of the shifted OECT characteristics.

We previously proposed a mechanism whereby de-doping with aliphatic amines involves a series of proton and electron transfer reactions to leave PEDOT:PSS in its de-doped state.^[29] Therefore, we studied both filling of PEDOT electronic states (electron transfer) and acid–base reactions with PSS (proton transfer) using ultraviolet–visible–near-infrared (UV–vis–NIR) absorption spectroscopy (Figure 3a–d) and x-ray photoelectron spectroscopy (XPS) (Figure 3e–h), respectively. From UV–vis–NIR, we observe an increase in the neutral-chain absorption band and a decrease in the polaron absorption band with increasing de-dopant concentration for each of the tested de-dopant molecules (Figure 3d). The decrease in neu-

tral chain absorption at high C_{amine} observed for DEMA and TAEA is attributed to the dilution of the absorber (PEDOT) in the film, which could explain the observed drop-off in mobility at high de-dopant concentrations (Figure 2g). The UV–vis–NIR results reveal a strong dependence between the concentration of de-dopant molecule and the degree of filling of the PEDOT neutral states and matches the trend for the conductivity of the “as de-doped” films (Figure 2e). Using XPS, we measured the nitrogen 1s (N1s) core electron energy level to determine the localized charge state of the amine functional groups. We observe distinct peaks at binding energies of ≈ 400 and ≈ 402 eV corresponding to neutral and positively charged amine functional groups, respectively^[23,31] (Figure 3e–g). By fitting the respective peaks, we find that the concentration of charged amine functional groups in the de-doped PEDOT:PSS films is $\approx 19.6 \pm 1.4$ mol% for all samples and de-dopant concentrations, while the concentration of sulfonate groups from PSS is $\approx 18.9 \pm 4.9$ mol%, indicating roughly a 1:1 ratio between charged amine functional groups and PSS units within the error of measurement (Figure 3h; Text S1, Supporting Information). This result indicates that the reaction is in an excess of amine at all measured concentrations; thus, the negative charge of most PSS units in the as-cast de-doped PEDOT:PSS films will be compensated by a positively charged amine group.

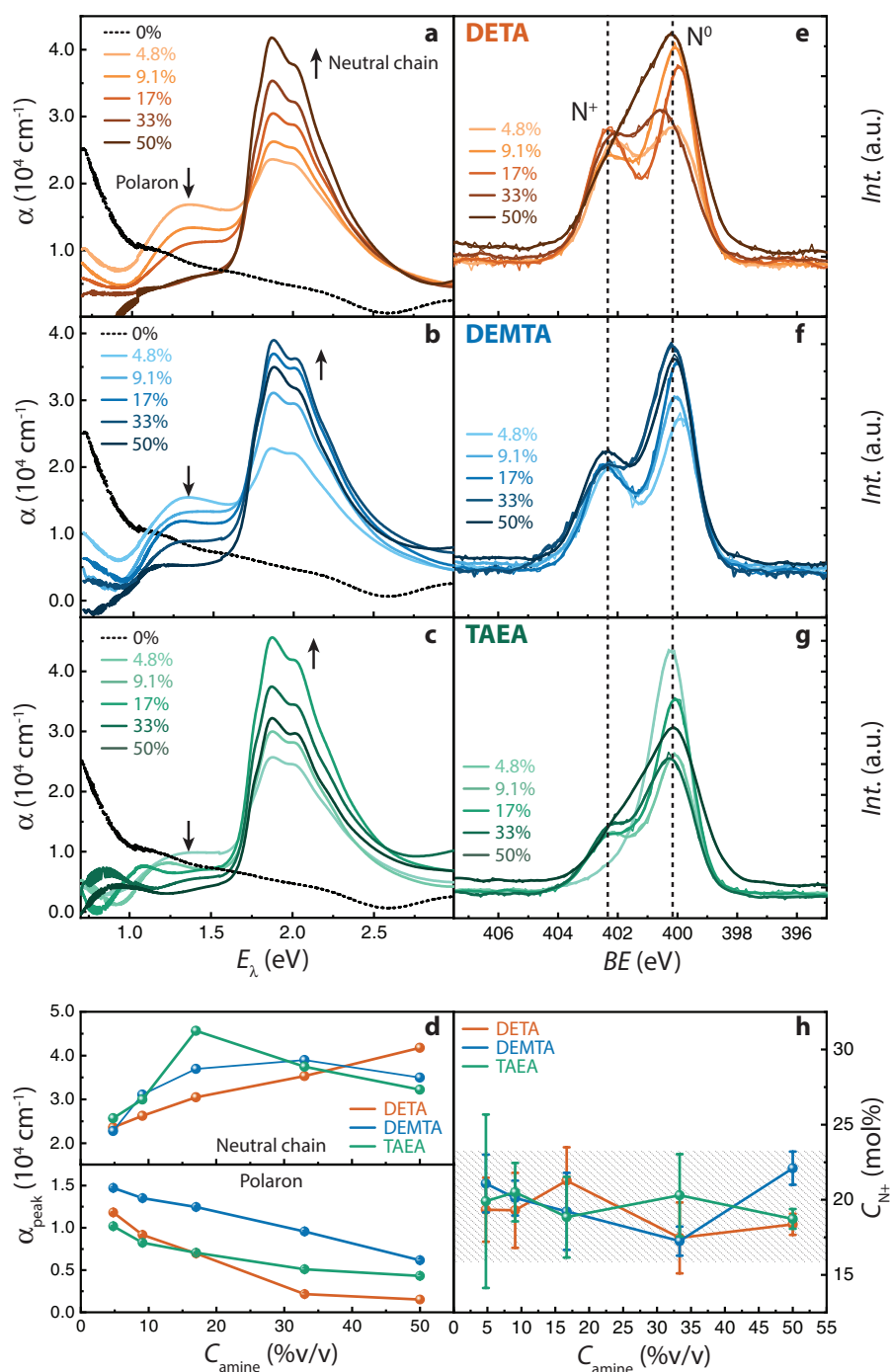


Figure 3. Characterization of electron and proton donation from molecular de-dopants. UV-vis-NIR absorption spectra for PEDOT:PSS films de-doped with varied concentrations of DETA (a), DEMTA (b), and TAEA (c) showing an increase in neutral-chain absorption (≈ 1.9 eV) and decrease in polaron absorption (≈ 1.3 eV) due to the filling of PEDOT electronic states. d) Quantification of the peak absorption for the neutral-chain and polaron transitions with increasing de-dopant. Carbon 1s normalized x-ray photoelectron spectra of the nitrogen 1s core electron for DETA (e), DEMTA (f), and TAEA (g) de-doped PEDOT:PSS showing the relative amount of charged ($\text{BE} \approx 402$ eV) and neutral ($\text{BE} \approx 400$ eV) amine functional groups. h) Comparison of the mole fraction of positively charged amines groups. Error bars in (d) and (h) denote the 95% confidence interval from the peak fitting procedures.

We propose the following mechanism to explain the behavior of the de-doped PEDOT:PSS blends: First, when the amine de-dopant is mixed with PEDOT:PSS solution, the sulfonate

and amine groups undergo an acid–base reaction followed by the formation of a cation–anion pair complex (Figure 4a). This reaction is evidenced by the release of heat following the

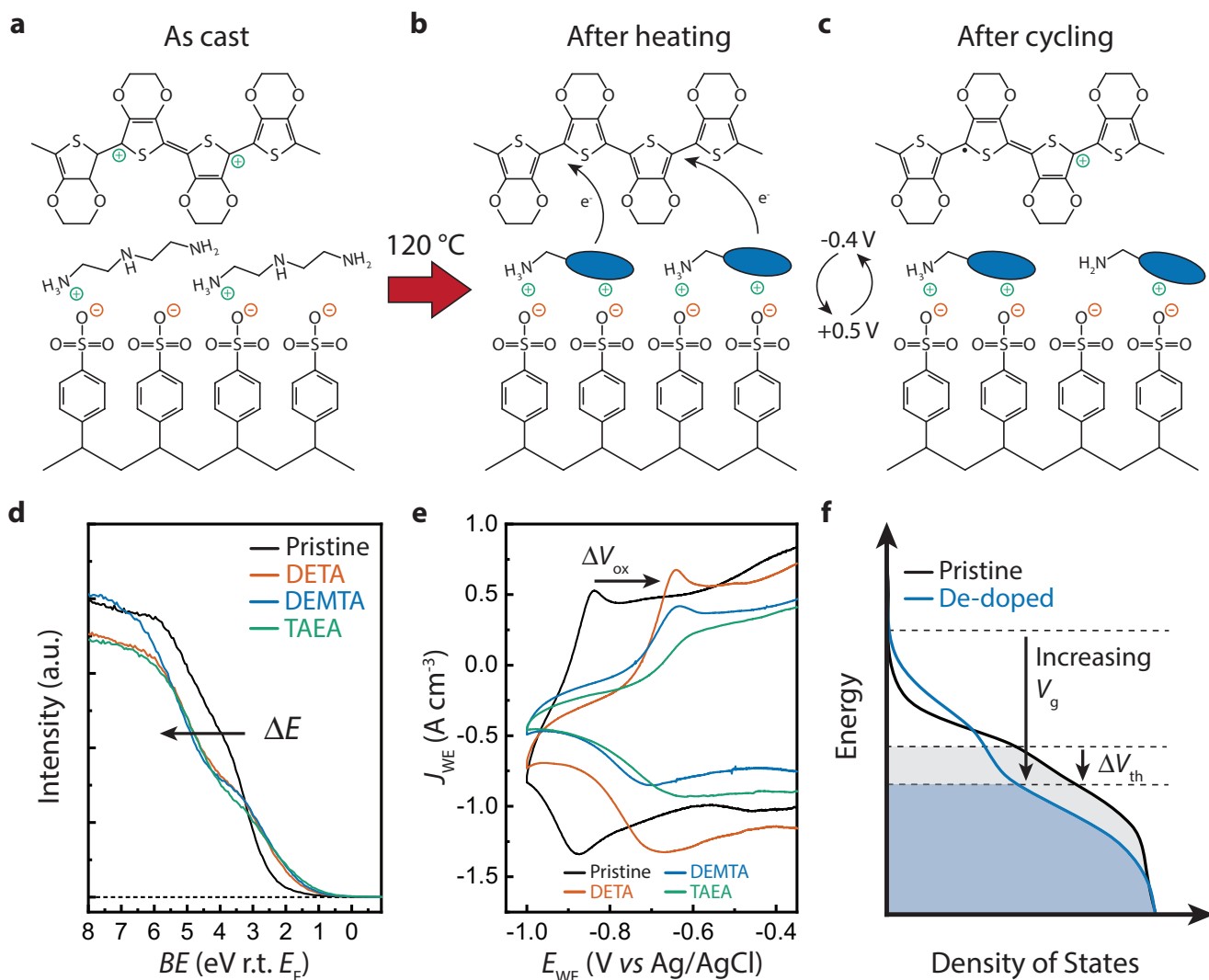


Figure 4. Proposed mechanism for shifted transistor characteristics of de-doped PEDOT:PSS devices. a–c) Schematics showing the chemical state of as cast (a), heat-treated (b), and electrochemically cycled (c) de-doped PEDOT:PSS films. Prior to heating, a) sulfonic acid groups transfer protons to amine groups and form an ion pair complex. Following heating, b) electrons are transferred from amines to the PEDOT backbone, leaving behind an unidentified charged amine species depicted as blue ovals. After electrochemical cycling, c) some charges remain on the PEDOT backbone. d) Ultra-violet photoelectron spectra of de-doped PEDOT:PSS (33% v/v) films following heat treatment. e) Oxidation onset from cyclic voltammetry showing a shift of the PEDOT oxidation peak for de-doped PEDOT:PSS films. This shift corresponds to the shift in the HOMO level of PEDOT, leading to the f) shift in OECT threshold voltage.

addition of the amine de-dopant and gelation at low amine concentrations (<4% v/v) (Figure S2, Supporting Information). The solution is then spin-coated and the resulting films are heated to 120 °C for 20 min. During heating, the electron transfer process from the neutral amine group to PEDOT is activated resulting in a rapid color change from a semi-transparent to a dark blue film (see Video S1, Supporting Information). Positively charged amine moieties formed following electron donation then compensate the negative charges of sulfonate groups which were previously compensating holes on PEDOT (Figure 4b). While the exact amine species generated by the electron donation reaction are not identified (see Figure S3, Supporting Information, for hypothesized structures based on ref. [29]), the XPS results suggest that positively charged amine groups are prevalent in the de-doped film.

Interestingly, during the first operation cycle, holes are not injected into the film until V_G reaches approx. -0.25 V, where the remaining unreacted amines oxidize completely; following the amine oxidation, holes are then injected into PEDOT causing an increase in drain current (Figure S4, Supporting Information). After the first electrochemical operation cycle, threshold voltages and conductivities of all de-dopants and concentrations remain similar (Figure 2d,f), indicating that a small concentration of holes remain on the PEDOT backbone following cycling (Figure 4c). These results indicate that after the first cycle the initial degree of de-doping of the as-cast films does not determine the resulting OECT device properties. However, the highest occupied molecular orbital (HOMO) level of the cycled films remains deeper than the HOMO level of pristine PEDOT:PSS, as observed by the shift in both the ultraviolet photoelectron

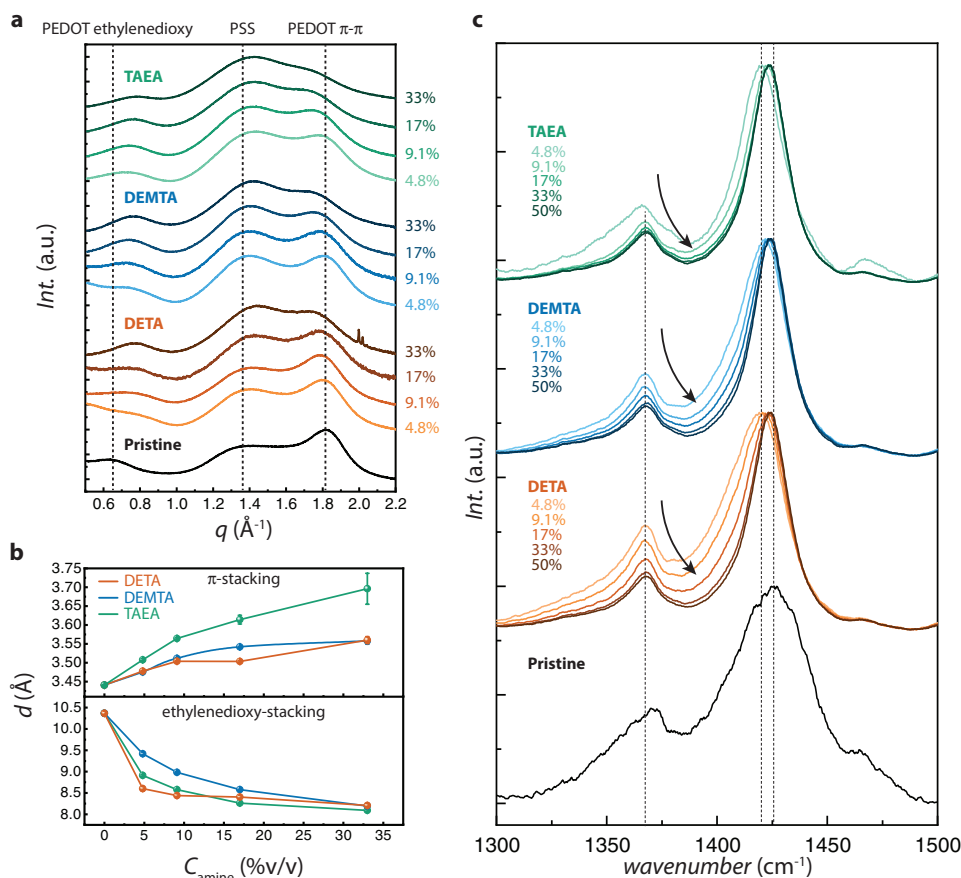


Figure 5. Structural characterization of de-doped PEDOT:PSS films. a) GIWAXS of de-doped PEDOT:PSS films with varied de-dopant concentration. Dashed lines in (a) denote characteristic peaks corresponding to (from left to right) PEDOT lamellar ethylenedioxy stacking, PSS amorphous halo, and PEDOT π - π stacking. b) Peak fitting results to find spacing distances d for the PEDOT π -stacking (top) and lamellar stacking (bottom) directions. Error bars denote the 95% confidence interval of the least squares fitting procedure. c) Raman spectroscopy of de-doped PEDOT:PSS films. Dashed lines show the peak shift of the PEDOT C=C stretch corresponding to a shift after de-doping with 4.8% v/v. Further de-doping shifts the peak toward the original position.

spectroscopy (UPS) spectra (Figure 4d) and the onset oxidation potential in cyclic voltammetry (Figure 4e). The shift in HOMO also explains the voltage shift in the transfer characteristics: as the gate voltage is swept from positive to negative, the mobile charges are not energetically favored until more negative potentials are reached compared to pristine PEDOT:PSS (Figure 4f). Furthermore, the tail of the valence states near the Fermi level in the de-doped PEDOT:PSS samples could indicate an increase in trap states following de-doping.^[32] Based on the experimental results, we hypothesize that the shift in the OECT threshold voltage is due to the compensation of sulfonate groups (dopants) by positively charged amine functional groups. The lower charge density of the polyanion (PSS) decreases the effective doping level of PEDOT. However, we found that the shift to enhancement-mode behavior cannot be achieved using a strong Brønsted–Lowry base alone (Figure S5, Supporting Information), indicating that the electron transfer reaction must also occur to achieve enhancement-mode OECTs. This result is consistent with previous work showing a more complicated cascading reaction, rather than a single proton transfer or electron transfer, is responsible for de-doping of PEDOT:PSS.^[29]

To understand the difference in device performance among varied de-dopant concentrations, we used grazing-incidence

wide-angle X-ray scattering (GIWAXS), atomic force microscopy (AFM), and Raman spectroscopy to study the molecular structure of the resulting films (Figure 4). From GIWAXS, we found that after de-doping the π - π stacking distance ($\approx 1.8 \text{ \AA}^{-1}$) expanded by 3.4–7.7% while the lamellar ethylenedioxy stacking ($\approx 0.7 \text{ \AA}^{-1}$) distance contracted by 21–22% for high de-dopant concentrations (33% v/v) (Figure 5a,b). This result is consistent with previous studies that have shown that ionic doping can lead to the opposite result (contracting π - π stacking and expanded lamellar stacking) in thiophene-based semiconductors.^[33,34] AFM phase contrast imaging showed more discrete phase boundaries as well as increased surface roughness when de-dopant molecules are included in solution (Figure S6 and Table S1, Supporting Information), which could lead to the lower mobilities observed for de-doped PEDOT:PSS OECTs.

Raman spectroscopy was used to investigate the structure of PEDOT (Figure 5c) using a 785 nm excitation laser which is off resonance with the neutral PEDOT chain (Figure S7, Supporting Information). We observe a prominent peak at ≈ 1400 – 1450 cm^{-1} which we assign to the C=C stretch of the PEDOT thiophene backbone.^[35] Pristine PEDOT:PSS exhibits a combination of quinoid (polaron) and benzoid (neutral chain) structures for the thiophene ring,^[36] resulting in a broad C=C

stretch vibration around 1425 cm^{-1} , and a C–C stretch around 1370 cm^{-1} . Upon addition of de-dopant at low concentration, the C=C peak first shifts to lower wavenumbers, but as the de-dopant concentration is increased from 4.8% v/v to 50% v/v, the peak shifts to higher wavenumbers. This behavior is similar to the Raman shifts observed for PEDOT with in situ spectroelectrochemical spectroscopy.^[36] The shift in the Raman spectrum is therefore attributed to the decrease in hole concentration on the PEDOT chains following molecular de-doping.

In this work, we have demonstrated a straightforward method to make enhancement-mode OECTs using a de-doped PEDOT:PSS channel cast from a single solution and a standard Ag/AgCl gate electrode. By utilizing a heat activated electron transfer de-doping mechanism, the channel material can be processed while PEDOT is still in its oxidized state, avoiding issues with solubility and processability associated with intrinsic (undoped) PEDOT. We show that all de-dopant concentrations used in this work give a similar shift in threshold voltage but optimizing the concentration results in improved transport of electronic charges and OECT performance. Furthermore, we show that by selecting the de-dopant molecular structure, we can improve the resulting film microstructure for improved electronic transport. The best performing enhancement-mode OECTs demonstrated here show a hole mobility of $2.17 \pm 0.06\text{ cm}^2\text{ V}^{-1}\text{ s}^{-1}$ (33% v/v DEMTA) and normalized peak transconductance $74 \pm 15\text{ S cm}^{-1}$ (20% v/v TAEA), which are not significantly lower than the performance metrics obtained with pristine PEDOT:PSS OECTs ($4.52 \pm 0.19\text{ cm}^2\text{ V}^{-1}\text{ s}^{-1}$ and $296 \pm 42\text{ S cm}^{-1}$, respectively).

The presented work demonstrates that amines can readily be used to adjust the operating potential of PEDOT:PSS OECTs by lowering the organic semiconductor HOMO level with respect to vacuum. We show that in order to shift PEDOT:PSS OECTs to enhancement-mode, the doping sulfonate units on the PSS component must be charge-compensated and electrons must be donated to neutralize the PEDOT backbone. Here, we only test small molecular weight amines as de-dopants, but it is expected that the same type of effect can be achieved using longer chain polyamines such as PEI. In future work, the molecular structure of de-dopants could be further optimized to enhance the microstructure of the spin-cast film by adjusting the relative solubility in the hydrophobic (PEDOT) and hydrophilic (PSS) phases of the polymer blend. Furthermore, the polymer/de-dopant blend could be optimized to shift V_{th} to larger negative voltages, lowering the channel current at $V_{\text{GS}} = 0\text{ V}$, for further improved enhancement-mode OECTs. Finally, we expect the de-doping strategy in this work to be generally applicable to organic semiconductor systems for either compensating p-type doping or for achieving n-type doping in other OMIEC materials.

Experimental Section

Materials and Device Fabrication: Device fabrication consisted of evaporating 5 nm Cr/50 nm Au on clean glass substrates (1 inch \times 1 inch) using a stainless-steel shadow mask to define the channel area. Next, the commercial PEDOT:PSS (Hereaus, Clevis PH 1000) aqueous dispersion was modified by adding 6 wt% ethylene glycol (EG, Sigma Aldrich) to enhance morphology and 1 wt% (3-glycidyloxypropyl)

trimethoxysilane (GOPS, Sigma Aldrich) as a crosslinker. Molecular de-dopants DETA, DEMTA, or TAEA (Sigma Aldrich) were added to the PEDOT:PSS dispersion at concentrations ranging from 4.8% v/v to 50% v/v. The dispersion was spun on the gold-coated glass slide at 1000 RPM for 2 min and baked at $120\text{ }^\circ\text{C}$ for 20 min. Polymer was removed from the substrate to define $1\text{ mm} \times 1\text{ mm}$ channels. A polydimethylsiloxane well (2 mm diameter) was fixed to the substrate to contain the aqueous electrolyte solution (100 mM NaCl). For cyclic voltammetry and UV–vis–NIR measurements, samples were coated onto transparent indium-tin oxide coated glass slides using the same conditions as above. For GIWAXS, Raman spectroscopy, and AFM measurements, samples were coated on n-doped silicon ($2\text{ cm} \times 2\text{ cm}$) with a native oxide layer using the same conditions as above.

Transistor Characterization: Transfer and output curves were measured with a Keithley 2612B source-measure unit with custom LabView code using a silver/silver chloride (Ag/AgCl) pellet as the gate electrode. During transfer curves, the drain voltage V_{D} was set to -0.1 V and the gate voltage V_{G} was swept from 0.5 to -0.4 V back to 0.5 V versus Ag/AgCl with voltage steps of 0.01 V at a sweep rate of 20 mV s^{-1} . This process was repeated three times to avoid artifacts in the data due to remaining unreacted de-dopant left in the film. During output curves, V_{D} was swept from 0.1 to -0.6 V in increments of 0.01 V at a sweep rate of 50 mV s^{-1} . This process was repeated for V_{G} spanning from $+0.5$ to -0.4 V versus Ag/AgCl with increments of 0.05 V. The saturation regime transfer curves are plotted by taking the current at $V_{\text{D}} = -0.6\text{ V}$ for each V_{G} of the resulting output curve.

UV–vis–NIR Absorption Spectroscopy: UV–vis–NIR absorption spectroscopy was carried out using a Cary 6000i photospectrometer. The transmittance was measured in dual beam mode to correct for the variance in the lamp flux, and a blank substrate was used as a 100% transmittance reference sample. The wavelength was swept from 1800 to 300 nm with 1 nm increments. Measurements were averaged until a signal-to-noise ratio of 10^4 was achieved.

XPS Measurements: XPS was carried out with a PHI Versaprobe III with an aluminum k_{α} X-ray source focused to a spot size $200\text{ }\mu\text{m} \times 200\text{ }\mu\text{m}$ under vacuum at a base pressure of 10^{-6} Pa . Films were pre-sputtered with an Argon Gas Cluster Ion Beam (GCIB) accelerated to 5 kV for 5 min prior to measurement to measure at a depth of $\approx 80\text{ nm}$ below the surface of the film.

GIWAXS and GISAXS Measurements: GIWAXS experiments were carried out at Stanford Synchrotron Radiation Lightsources (SSRL) at beamline 11-3 using an area CCD detector (Rayonix MAR 225) at a distance of 316.386 mm (calibrated with LaB_6 standard reference), an incident beam energy of 12.73 keV, and an incidence angle of 0.1° . The beam path was filled with helium to avoid air scattering between the sample and detector. The data reduction from 2D to 1D data was performed using Nika,^[37] Irena,^[38] and WAXStools,^[39] and Gaussian peak fitting was performed using a least-squares fitting algorithm in MatLab.

Raman Spectroscopy: Raman spectra were taken using a Horiba XploRA confocal Raman microscope with a 785 and 638 nm excitation laser source. A $100 \times 0.6\text{ NA}$ objective was used to give diffraction-limited spot sizes of $\approx 650\text{ nm}$ (785 nm laser) and $\approx 530\text{ nm}$ (638 nm laser). A laser power of 2.23 mW for the 785 nm laser and 0.121 mW for the 638 nm laser were used.

UPS Measurements: UPS was carried out on a multi-chamber ESCALAB II system, using -6 V bias and the He I line (21.22 eV) for excitation.

Thickness Measurements: Sample thicknesses were measured using a Bruker Dektak XT profilometer with 1 mg of force and a scan rate of $35\text{ }\mu\text{m s}^{-1}$. Sample thickness was averaged over five individual measurements at different locations of the film.

Supporting Information

Supporting Information is available from the Wiley Online Library or from the author.

Acknowledgements

The authors would like to thank Camila Cendra and Dr. Christopher Tassone for fruitful discussions about X-ray scattering. A.S. and S.T.K. acknowledge financial support from the National Science Foundation and the Semiconductor Research Corporation, E2CDA Type II Award #1739795 and DMR Award #1808401. Additionally, S.T.K. acknowledges the Stanford Graduate Fellowship fund grant number 6037395 for support. D.Z. and A.S. acknowledge the Stanford SystemX Seed Grant for support. This work was in part performed at the Stanford Nano Shared Facilities (SNSF) and the nano@Stanford (SNF) labs, which are supported by the National Science Foundation as part of the National Nanotechnology Coordinated Infrastructure under award ECCS-1542152. Part of this work was performed at the Stanford Synchrotron Radiation Laboratory, SLAC National Accelerator Laboratory, which is supported by the U.S. Department of Energy, Office of Science, Office of Basic Energy Sciences under Contract No. DE-AC02-76SF00515. Y.v.d.B. gratefully acknowledges funding from the European Union's Horizon 2020 Research and Innovation Programme, grant agreement No. 802615. C.H.L.W. and R.A.J.J. acknowledge funding from the Netherlands Organisation for Scientific Research (Spinoza prize). T.v.d.P. acknowledges funding from the Ministry of Education, Culture and Science (Gravity program 024.001.035).

Conflict of Interest

The authors declare no conflict of interest.

Keywords

aliphatic amines, bioelectronics, enhancement-mode transistor, molecular doping, organic electrochemical transistor, poly(ethylenedioxythiophene):poly(styrene sulfonate)

Received: January 13, 2020

Revised: February 28, 2020

Published online: March 23, 2020

- [1] W. Gao, S. Emaminejad, H. Y. Y. Nyein, S. Challa, K. Chen, A. Peck, H. M. Fahad, H. Ota, H. Shiraki, D. Kiriya, D. H. Lien, G. A. Brooks, R. W. Davis, A. Javey, *Nature* **2016**, 529, 509.
- [2] E. Bihar, Y. Deng, T. Miyake, M. Saadaoui, G. G. Malliaras, M. Rolandi, *Sci. Rep.* **2016**, 6, 2.
- [3] O. Parlak, S. T. Keene, A. Marais, V. F. Curto, A. Salleo, *Sci. Adv.* **2018**, 4, eaar2904.
- [4] S. T. Keene, D. Fogarty, R. Cooke, C. D. Casadevall, A. Salleo, O. Parlak, *Adv. Healthcare Mater.* **2019**, 8, 1901321.
- [5] D. Khodagholy, J. N. Gelinias, T. Thesen, W. Doyle, O. Devinsky, G. G. Malliaras, G. Buzsáki, *Nat. Neurosci.* **2015**, 18, 310.
- [6] D. Khodagholy, T. Doublet, P. Quilichini, M. Gurfinkel, P. Leleux, A. Ghestem, E. Ismailova, T. Hervé, S. Sanaur, C. Bernard, G. G. Malliaras, *Nat. Commun.* **2013**, 4, 1575.
- [7] J. Rivnay, H. Wang, L. Fenno, K. Deisseroth, G. G. Malliaras, *Sci. Adv.* **2017**, 3, e1601649.
- [8] D. Pani, A. Dessi, J. F. Saenz-Cogollo, G. Barabino, B. Fraboni, A. Bonfiglio, *IEEE Trans. Biomed. Eng.* **2016**, 63, 540.
- [9] P. Lin, F. Yan, J. Yu, H. L. W. Chan, M. Yang, *Adv. Mater.* **2010**, 22, 3655.
- [10] J. Rivnay, M. Ramuz, P. Leleux, A. Hama, M. Huerta, R. M. Owens, *Appl. Phys. Lett.* **2015**, 106, 043301.
- [11] F. Santoro, Y. van de Burgt, S. T. Keene, B. Cui, A. Salleo, *ACS Appl. Mater. Interfaces* **2017**, 9, 39116.
- [12] Y. van de Burgt, E. Lubberman, E. J. Fuller, S. T. Keene, G. C. Faria, S. Agarwal, M. J. Marinella, A. A. Talin, A. Salleo, *Nat. Mater.* **2017**, 16, 414.
- [13] Y. van de Burgt, A. Melianas, S. T. Keene, G. Malliaras, A. Salleo, *Nat. Electron.* **2018**, 1, 386.
- [14] E. J. Fuller, S. T. Keene, A. Melianas, Z. Wang, S. Agarwal, Y. Li, Y. Tuchman, C. D. James, M. J. Marinella, J. J. Yang, A. Salleo, A. A. Talin, *Science* **2019**, 364, 570.
- [15] J. Rivnay, S. Inal, A. Salleo, R. M. Owens, M. Berggren, G. G. Malliaras, *Nat. Rev. Mater.* **2018**, 3, 17086.
- [16] C. M. Proctor, J. Rivnay, G. G. Malliaras, *J. Polym. Sci., Part B: Polym. Phys.* **2016**, 54, 1433.
- [17] A. V. Volkov, K. Wijeratne, E. Mitraka, U. Ail, D. Zhao, K. Tybrandt, J. W. Andreasen, M. Berggren, X. Crispin, I. V. Zozoulenko, *Adv. Funct. Mater.* **2017**, 27, 1700329.
- [18] J. Rivnay, P. Leleux, M. Ferro, M. Sessolo, A. Williamson, D. A. Koutsouras, D. Khodagholy, M. Ramuz, X. Strakosas, R. M. Owens, C. Benar, J.-M. Badier, C. Bernard, G. G. Malliaras, *Sci. Adv.* **2015**, 1, e1400251.
- [19] E. Stavrinidou, P. Leleux, H. Rajaona, D. Khodagholy, J. Rivnay, M. Lindau, S. Sanaur, G. G. Malliaras, *Adv. Mater.* **2013**, 25, 4488.
- [20] D. Khodagholy, J. Rivnay, M. Sessolo, M. Gurfinkel, P. Leleux, L. H. Jimison, E. Stavrinidou, T. Herve, S. Sanaur, R. M. Owens, G. G. Malliaras, *Nat. Commun.* **2013**, 4, 2133.
- [21] S. Inal, G. G. Malliaras, J. Rivnay, *Nat. Commun.* **2017**, 8, 1767.
- [22] Y. Xuan, M. Sandberg, M. Berggren, X. Crispin, *Org. Electron.* **2012**, 13, 632.
- [23] S. T. Keene, A. Melianas, Y. van de Burgt, A. Salleo, *Adv. Electron. Mater.* **2019**, 5, 1800686.
- [24] W. J. Dally, J. W. Poulton, *Digital Systems Engineering*, Cambridge University Press, Cambridge, UK **1998**, p. 158.
- [25] D. A. Johns, K. Martin, *Analog Integrated Circuit Design*, John Wiley and Sons, New York **1997**, p. 28.
- [26] S. Fabiano, S. Braun, X. Liu, E. Weverberghs, P. Gerbaux, M. Fahlman, M. Berggren, X. Crispin, *Adv. Mater.* **2014**, 26, 6000.
- [27] S. E. Doris, A. Pierre, R. A. Street, *Adv. Mater.* **2018**, 30, 1706757.
- [28] C. B. Nielsen, A. Giovannitti, D. T. Sbircea, E. Bandiello, M. R. Niazi, D. A. Hanifi, M. Sessolo, A. Amassian, G. G. Malliaras, J. Rivnay, I. McCulloch, *J. Am. Chem. Soc.* **2016**, 138, 10252.
- [29] T. P. A. van der Pol, S. T. Keene, B. W. H. Saes, S. C. J. Meskers, A. Salleo, Y. van de Burgt, R. A. J. Janssen, *J. Phys. Chem. C* **2019**, 123, 24328.
- [30] D. A. Bernards, G. G. Malliaras, *Adv. Funct. Mater.* **2007**, 17, 3538.
- [31] Z. Lin, J. Chang, J. Zhang, C. Jiang, J. Wu, C. Zhu, *J. Mater. Chem. A* **2014**, 2, 7788.
- [32] Z. Shang, T. Heumueller, R. Prasanna, G. F. Burkhard, B. D. Naab, Z. Bao, M. D. McGehee, A. Salleo, *Adv. Energy Mater.* **2016**, 6, 1601149.
- [33] J. O. Guardado, A. Salleo, *Adv. Funct. Mater.* **2017**, 27, 1701791.
- [34] C. Cendra, A. Giovannitti, A. Savva, V. Venkatraman, I. McCulloch, A. Salleo, S. Inal, J. Rivnay, *Adv. Funct. Mater.* **2019**, 29, 1807034.
- [35] W. C. Tsoi, D. T. James, J. S. Kim, P. G. Nicholson, C. E. Murphy, D. D. C. Bradley, J. Nelson, J. S. Kim, *J. Am. Chem. Soc.* **2011**, 133, 9834.
- [36] S. Garreau, G. Louarn, J. P. Buisson, G. Froyer, S. Lefrant, *Macromolecules* **1999**, 32, 6807.
- [37] J. Ilavsky, *J. Appl. Crystallogr.* **2012**, 45, 324.
- [38] J. Ilavsky, P. R. Jemian, *J. Appl. Crystallogr.* **2009**, 42, 347.
- [39] S. D. Oosterhout, V. Savikhin, J. Zhang, Y. Zhang, M. A. Burgers, S. R. Marder, G. C. Bazan, M. F. Toney, *Chem. Mater.* **2017**, 29, 3062.